

Comparing the transitional behaviour of kaolinite and bentonite suspension flows

Jaco H. Baas,^{1*} James L. Best² and Jeff Peakall³

¹ School of Ocean Sciences, Bangor University, Bangor, Wales, UK

² Departments of Geology, Geography and GIS, Mechanical Science and Engineering and Ven Te Chow Hydrosystems Laboratory, University of Illinois at Urbana-Champaign, Champaign, IL USA

³ School of Earth and Environment, University of Leeds, Leeds, UK

Received 30 October 2015; Revised 22 February 2016; Accepted 12 April 2016

*Correspondence to: Jaco H. Baas, School of Ocean Sciences, Bangor University, Menai Bridge, Isle of Anglesey, LL59 5AB, Wales, UK. E-mail: j.baas@bangor.ac.uk
This is an open access article under the terms of the Creative Commons Attribution License, which permits use, distribution and reproduction in any medium, provided the original work is properly cited.

ESPL

Earth Surface Processes and Landforms

ABSTRACT: Past research has demonstrated the dramatic effects that variations in suspended clay can have on the properties of flow by producing a range of transitional flows between turbulent and laminar states, depending on clay concentration and fluid shear. Past studies have been restricted to kaolinite flows, a clay mineral that has relatively weak cohesive properties. This paper extends these studies to suspension flows of bentonite, a clay mineral that attains higher viscosities at far lower volumetric concentrations within a flow. The results show that the types of transitional flow behaviour recognized in past studies can also be found in bentonite suspension flows, but at lower suspended sediment concentrations, thus demonstrating an even more dramatic effect on flow properties, and potentially on sediment transport and resulting bed morphology, than kaolinite flows. The paper proposes new stability diagrams for the phase space of bentonite flows and compares these to past work on kaolinite suspension flows. These new data suggest that the transitional-flow Reynolds number can be used to delineate the types of transitional flow across different clay types and assess modern and ancient clay-suspension flows. © 2016 The Authors. Earth Surface Processes and Landforms published by John Wiley & Sons Ltd.

KEYWORDS: flume experiments; transitional flow; cohesion; bentonite; kaolinite

Introduction

Clay-mineral laden currents with a transient turbulent behaviour (or transitional clay flows; Wang and Plate, 1996; Baas and Best, 2002), have unique dynamic properties that set them apart from turbulent flows and laminar, turbulence-free flows at low and high suspended sediment concentrations, respectively (Baas and Best, 2002; Baas *et al.*, 2009). Baas *et al.* (2009) demonstrated that a range of transitional flows can be recognized that exhibit both turbulence enhancement, such as in turbulence-enhanced transitional flows and in the basal region of lower transitional plug flows, and turbulence attenuation, which characterizes the plug flow region of lower transitional plug flows and appears throughout upper transitional plug flows. The sedimentary signature of such transient turbulent behaviour has been recognized in a wide range of environmental flows, including rivers, density currents in lakes, lahars, high-density estuarine currents, and sediment gravity flows in the deep oceans (e.g. Amos *et al.*, 2003; Sylvester and Lowe, 2004; Kleinhans and Grasmeijer, 2006; Alexander *et al.*, 2010; Hansen *et al.*, 2011; Chang and Chun, 2012; Carling, 2013; Plint, 2014; La Croix and Dashtgard, 2014; Chang *et al.*, 2015; Harazim and McIlroy, 2015; Jablonski and Dalrymple, 2016). The original model for turbulence modulation in clay-laden flows, proposed by Baas and Best (2002) and Baas *et al.* (2009), and summarized in a clay flow phase diagram,

was based on suspensions laden with kaolin clay. This model shows that even small amounts of kaolinite (well below 1% by volume) are sufficient to cause turbulence modulation through flocculation and gelling of clay particles, especially at low flow velocities. This rheological behaviour is remarkable, considering that kaolinite is a clay mineral with weak cohesive properties (Wan, 1982). Herein, we show that clay minerals with stronger cohesive properties can change the flow properties at even lower suspended clay concentrations than kaolinite. The present paper presents results from a new series of laboratory experiments investigating turbulence modulation in steady, uniform flows laden with highly cohesive bentonite clay. The objectives of this research were: (1) to investigate transitional flow behaviour in steady, uniform currents laden with bentonite clay, based on detailed records of velocity, turbulence intensity, and suspended sediment concentration; (2) to contrast the transitional behaviour of kaolinite and bentonite flows; and (3) to test the robustness of the clay-flow phase diagram of Baas *et al.* (2009) for bentonite clay.

Transitional Clay Flows

The boundary layer of clear-water turbulent flows that move over a flat surface is characterized by a logarithmic profile of

the downstream component of velocity, and turbulence intensities that are highest in the zone of near-bed shear and gradually decrease upward. As fine cohesive kaolinite is added to a turbulent flow (TF), the fluid begins to display a range of transitional behaviours, because turbulence becomes modulated by the presence of the cohesive particles (Baas and Best, 2002; Baas *et al.*, 2009). This turbulence modulation has four stages (Figures 1, 2): (i) drag reduction or turbulence-enhanced transitional flow (TETF); (ii) lower transitional plug flow (LTPF); (iii) upper transitional plug flow (UTPF); (iv) quasi-laminar plug flow (QLPF) (Baas *et al.*, 2009, 2016). TETF is characterized by turbulence intensities, expressed by the root-mean square values of the downstream component of velocity, $RMS(u')$, that are higher than in clear-water TF (Figures 2a–2e). The source of this turbulence enhancement has been related to drag reduction in the boundary layer, which causes a thickening of the viscous sublayer and maximum shear at the top of this sublayer (e.g. Gust, 1976; Caldwell and Chriss, 1979; Best and Leader, 1993; Baas *et al.*, 2016). Time-series of the streamwise velocity at the height of maximum shear show distinct, second-scale, ‘saw-tooth’-shaped patterns that represent Kelvin–Helmholtz

instabilities that are particularly well expressed at higher clay concentrations in LTPF, because higher-frequency velocity fluctuations are suppressed in this type of flow (Figure 2f). LTPF is different from TETF in that shear in the outer flow is insufficient to break up the clay flocs, resulting in the development of a plug flow in which downstream velocity is invariant with depth (Figures 2a–2c). Below this plug, the velocity time-series show short negative spikes in streamwise velocity that have been interpreted as packets of low velocity fluid shed off the top of the Kelvin–Helmholtz instabilities (Figure 2g; Baas and Best, 2002; Baas *et al.*, 2009). The combination of turbulence enhancement in the lower part of LTPF and turbulence attenuation in the upper part of LTPF results in steep vertical gradients of downstream velocity and $RMS(u')$ (Figures 2a–2c). If the near-bed suspended clay concentration is high enough to prevent turbulence from breaking the bonds between clay particles, turbulence becomes attenuated through the entire flow. Such UTPFs are characterized by low near-bed $RMS(u')$ and a plug flow zone that thickens down from the water surface (Figures 2a–2c, h). A pervasive network of clay particle bonds, i.e. a gel, typifies QLPF. Kaolinite-laden QLPFs have a thin basal

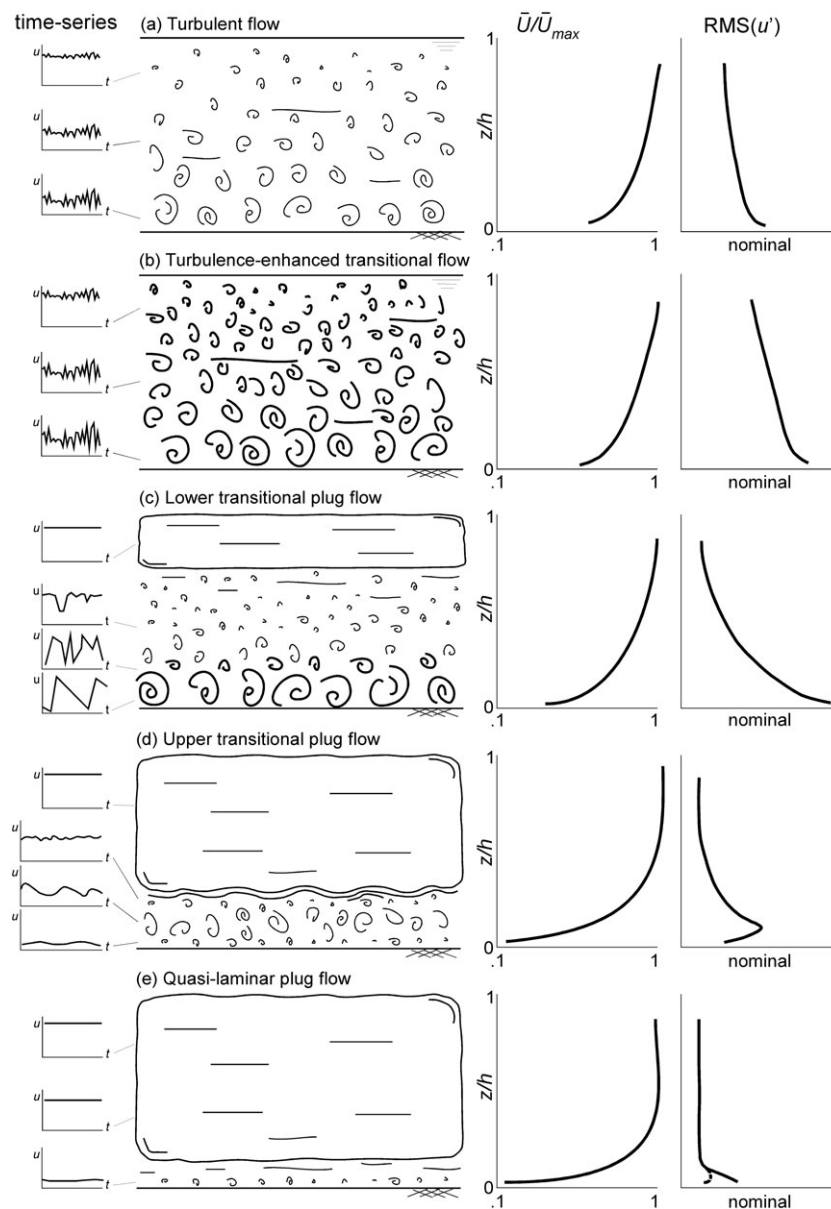


Figure 1. Schematic models of turbulent, transitional and quasi-laminar clay flows over a smooth, flat bed. Characteristic velocity time series at various heights in the flows are given on the left-hand side. The graphs to the right of the models represent characteristic vertical profiles of dimensionless downstream velocity (U_{max} is maximum flow velocity) and $RMS(u')$. Modified after Baas *et al.* (2009).

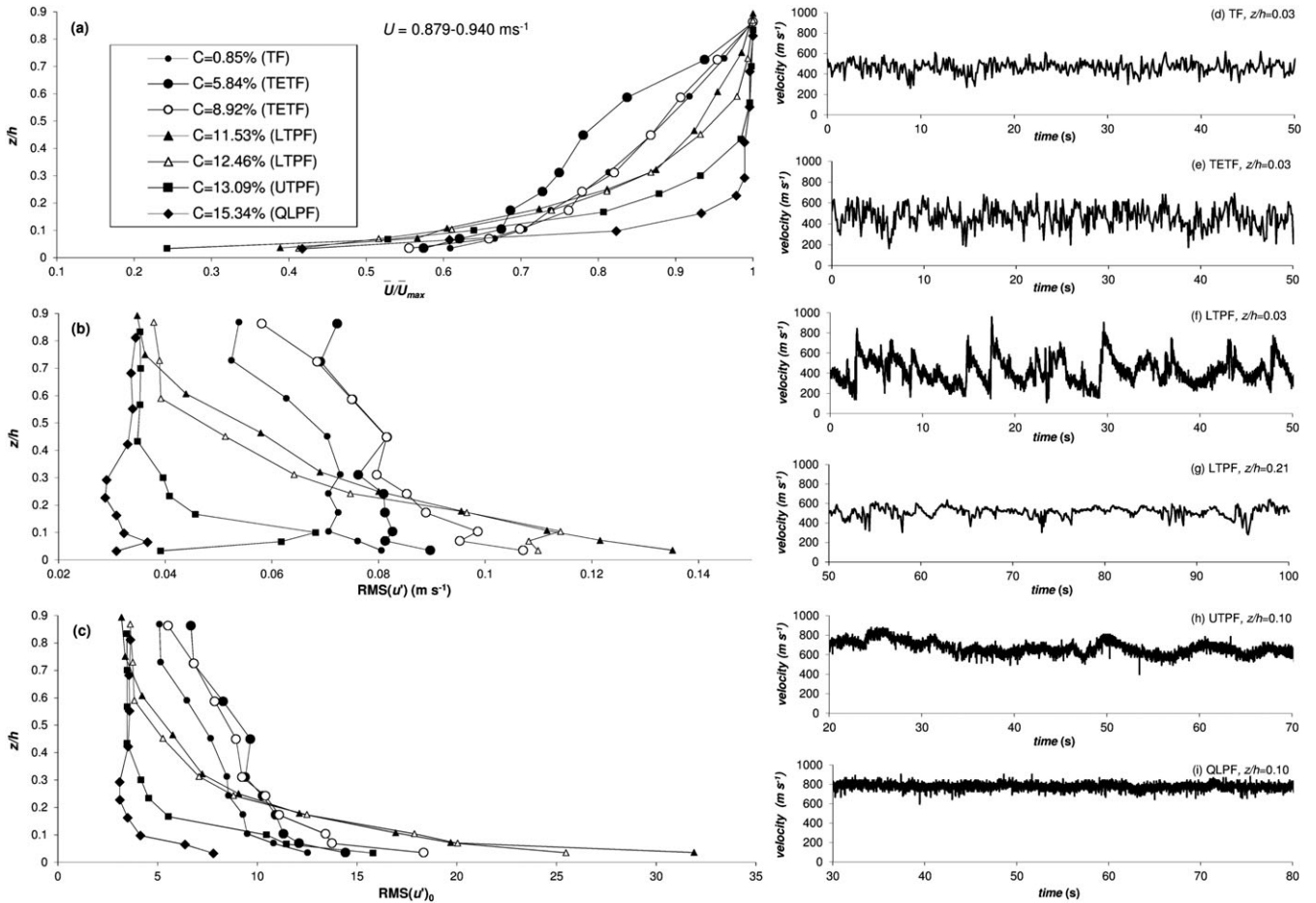


Figure 2. Representative examples of vertical profiles of (a) downstream flow velocity, (b) RMS(u') and (c) RMS(u')₀, and (d–i) time-series of downstream velocity in kaolinite flows. (a–c) Different flow types for a narrow range of velocities, $U = 0.0879–0.904 \text{ m s}^{-1}$. (d–f, h, i) Velocity near-bed time-series for turbulent flow (TF), turbulence-enhanced transitional flow (TETF), lower transitional plug flow (LTPF), upper transitional plug flow (UTPF), and quasi-laminar plug flow (QLPF), respectively. (g) A characteristic velocity time-series for the top of an internal shear layer in LTPF.

shear layer with minimal turbulence production, but the bulk of these flows consists of a plug flow in which velocity fluctuations and vertical exchange of fluid and sediment are negligible (Figures 2a–2c, i).

Baas *et al.* (2009) proposed a phase diagram for clay flows laden with kaolinite that delineates the boundaries between TF, TETF, LTPF, UTPF, and QLPF for different combinations of depth-averaged flow velocity and suspended sediment concentration, and, in non-dimensional form, for Froude number, Fr , and transitional-flow Reynolds number, Re_{TF} (Figure 3):

$$Fr = \frac{U}{\sqrt{gh}} \tag{1}$$

$$Re_{TF} = \frac{Uz_p\rho}{\eta} \tag{2}$$

where U is depth-averaged flow velocity, h is flow depth, g is acceleration due to gravity, ρ is flow density, η is the dynamic viscosity of the flow, and z_p is the thickness of the flow region below the base of the plug flow. In Equation 2, z_p is used instead of flow depth, because the largest length scales of turbulence within the transitional and laminar clay flows are limited by the distance between the lower flow boundary and the base of the plug-flow region. This non-dimensional phase diagram was used by Baas *et al.* (2009) to distinguish between the main clay flow types,

based on narrow ranges of transitional-flow Reynolds numbers: (1) $Re_{TF} = 55,000 \pm 20,000$ separates TF from TETF; (2) $Re_{TF} = 28,100 \pm 6100$ separates TETF from LTPF; (3) $Re_{TF} = 12,000 \pm 3400$ separates LTPF from UTPF; and (4) $Re_{TF} = 7000 \pm 2400$ separates UTPF from QLPF. The phase diagram of Baas *et al.* (2009) also shows a flow type at transitional-flow Reynolds numbers smaller than 10,000 and Froude numbers below 0.3, where the clay flows are unstable and deposition occurred within the duration of the experiments (labelled 'Deposition' in Figure 3). The present paper investigates if this diagram can be used to interpret the behaviour of transitional flows that carry a clay mineral with stronger cohesive properties, and how such flows may influence the stability space of these clay flow types.

Experimental Setup and Methodology

Forty-nine laboratory experiments were conducted using an 8.75 m long and 0.3 m wide slurry flume in the Sorby Environmental Fluid Dynamics Laboratory, University of Leeds, UK (Figure 4; Table I). The principal aim of these experiments was to extend the parameter space of the laboratory experiments conducted by Baas *et al.* (2009) that examined changes in flow properties of steady, uniform, kaolinite-laden flows as a function of suspended clay concentration and flow forcing to bentonite-laden flows. This new series of experiments used the same experimental setup and methodology as Baas *et al.* (2009), which are summarized below. Mixtures of fresh water and cohesive bentonite clay, at depth-averaged volumetric

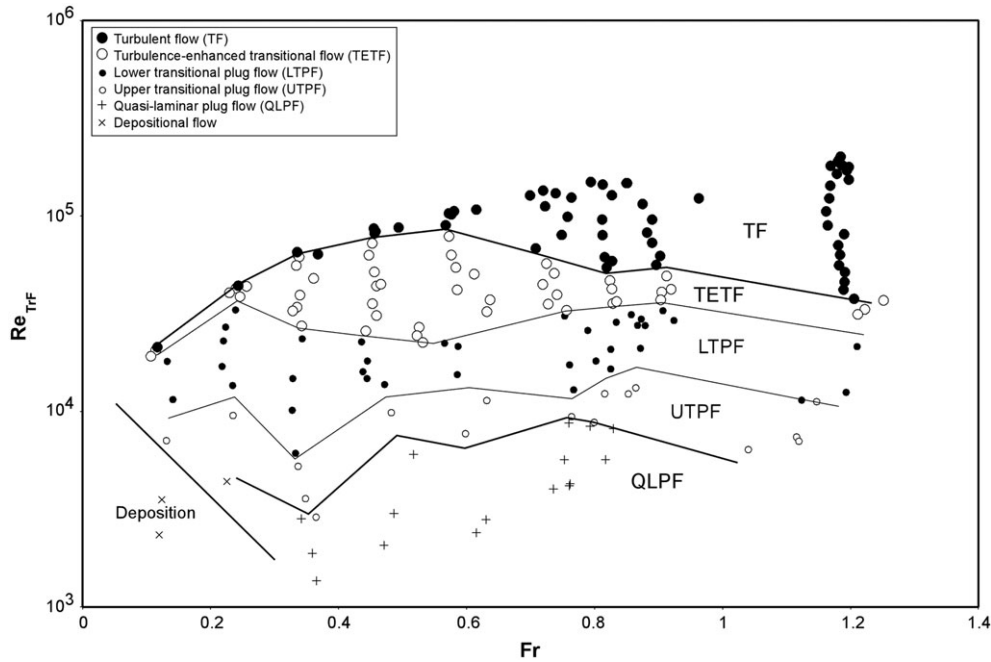


Figure 3. Phase diagram for kaolinite flows moving over a flat, smooth, fixed boundary, plotted using the Froude number, Fr , and transitional-flow Reynolds number, Re_{TF} . Modified after Baas *et al.* (2009).

concentrations ranging from 0.04% to 8.63%, were circulated through the flume by means of a slurry pump, whose open structure minimizes flow disturbance. The bentonite clay used in the experiments had an undispersed and dispersed median particle diameter, D_{50} , of 0.017 mm and 0.013 mm, respectively (Figure 5). This is comparable to the median diameter of 0.009 mm for the kaolinite used by Baas *et al.* (2009), suggesting that the effect of differences in grain size on flow behaviour was small. The flows moved over a smooth, featureless bed along the entire length of the flume at depth-averaged flow velocities, U , ranging from 0.280 m s^{-1} to 1.418 m s^{-1} . These average values were calculated by fitting downstream velocities recorded by means of ultrasonic Doppler velocity profilers (UDVP; see Takeda, 1991; Best *et al.*, 2001, for details) to the logarithmic law for wall-bounded shear flows (e.g. Van Rijn, 1990), or the Coles' wake function (Coles, 1956) for flows with a well-developed plug flow region. UDVPs quantify flow velocity by determining the Doppler shift in ultrasound frequency as small particles pass through a measurement volume, and thus rely on the reasonable assumption that the clay particles move at the same velocity as the fluid. Each UDVP acquired simultaneous velocity data along a profile of up to 128 points along the axis of the ultrasound beam, which in the present experiments extended up to 0.105 m from the probe head. No velocities were recorded in the proximal 0.012 m, where the stagnation of flow by the UDVP was found to be unacceptably large. Velocity data were obtained at nine or ten different heights, z , above the bed (between $z=0.005 \text{ m}$

and $z=0.125 \text{ m}$). The UDVPs collected velocity data for durations of 75 to 120 seconds at a temporal resolution of 83 to 133 Hz (Table I). The standard deviation of the temporal mean downstream flow velocity, $RMS(u')$, where RMS denotes root-mean-square and u' is the fluctuation in downstream velocity equal to $u - U_t$, was calculated from the time series of instantaneous velocity data at each measurement height:

$$RMS(u') = \sqrt{\frac{1}{n} \sum_{i=1}^n (u_i - U_t)^2} \quad (3)$$

where n is the number of velocity measurements, and u is the excursion of velocity from the time-averaged velocity U_t . A dimensionless measure for turbulence intensity was defined as:

$$RMS(u')_0 = \frac{RMS(u')}{U} \cdot 100 \quad (4)$$

Table I lists the depth-averaged and maximum flow velocities, Froude numbers and transitional-flow Reynolds numbers derived from U (following procedures described in Baas *et al.* 2009). Flow depths were between 0.130 and 0.160 m.

Following Wan (1982), the dynamic viscosity, η , and the yield strength, τ_y , of the bentonite suspensions were approximated from the measured suspended-sediment concentrations as follows:

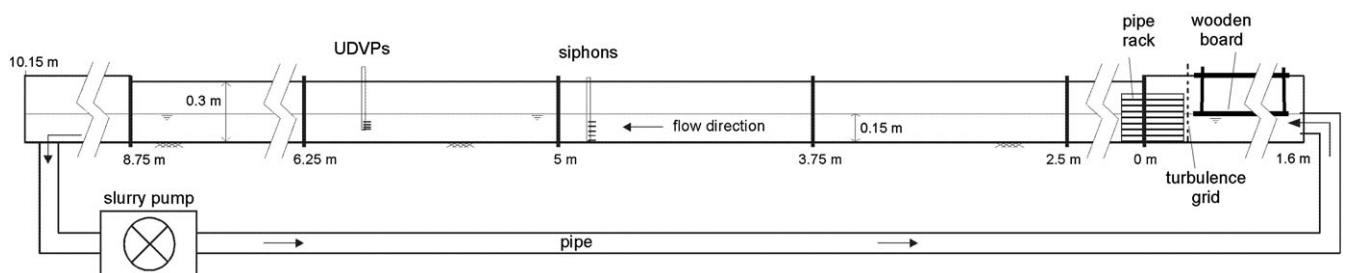


Figure 4. Schematic diagram of the experimental setup. UDVP, ultrasonic Doppler velocity profilers.

Table 1. Experimental parameters

Run	Duration (s)	<i>T</i> (°C)	<i>C</i> (vol%)	<i>C</i> (g l ⁻¹)	η (10 ⁻³ Ns m ⁻²)	τ_y (N m ⁻²)	<i>h</i> (m)	<i>z_p</i> (m)	<i>f</i> (UDVP) (Hz)	<i>U</i> (m s ⁻¹)	<i>U_{max}</i> (m s ⁻¹)	<i>Fr</i> (-)	<i>Re_{TF}</i> (-)	Slope × 10 ⁻³	Flow regime
1-1	120	20.7	0.04	1.1	1.004	0.000	0.156	0.156	83	0.304	0.345	0.25	47200	0.18	TF
1-2	120	20.7	0.13	3.4	1.018	0.000	0.158	0.158	83	0.305	0.348	0.25	47478	0.18	TF
1-3	120	22.1	0.26	6.7	1.043	0.000	0.160	0.160	83	0.307	0.349	0.24	47250	0.18	TF
1-4	120	22	0.46	11.9	1.091	0.000	0.159	0.159	83	0.312	0.359	0.25	45767	0.18	TETF
1-5	120	21.3	0.61	15.9	1.133	0.000	0.150	0.150	83	0.284	0.344	0.23	37982	0.18	TETF
1-6	120	21.4	0.93	24.1	1.229	0.001	0.156	0.156	83	0.310	0.368	0.25	39922	0.18	TETF
1-7	120	22.5	1.27	32.9	1.343	0.002	0.156	0.156	83	0.304	0.363	0.25	36012	0.18	TETF
1-8	120	20.7	1.73	44.9	1.512	0.007	0.158	0.158	83	0.280	0.324	0.22	30028	0.18	TETF
1-9	120	22.7	2.32	60.3	1.751	0.021	0.155	0.155	83	0.316	0.378	0.26	29003	0.18	TETF
1-10	120	22.7	2.83	73.6	1.972	0.043	0.158	0.158	83	0.314	0.377	0.25	26257	0.18	TETF
1-11	120	23	3.74	97.1	2.394	0.120	0.156	0.075	83	0.318	0.370	0.26	10553	0.18	LTPF
2-1	87	20.7	0.05	1.4	1.006	0.000	0.151	0.151	115	0.595	0.678	0.49	89392	0.29	TF
2-2	87	20.7	0.17	4.5	1.026	0.000	0.154	0.154	115	0.592	0.675	0.48	89046	0.29	TF
2-3	87	22.2	0.32	8.3	1.058	0.000	0.156	0.156	115	0.586	0.663	0.47	86831	0.29	TF
2-4	87	22.1	0.57	14.8	1.121	0.000	0.155	0.155	115	0.594	0.672	0.48	82852	0.29	TF
2-5	87	21.3	0.83	21.6	1.198	0.000	0.144	0.144	115	0.638	0.727	0.54	77720	0.29	TETF
2-6	87	21.3	1.22	31.8	1.327	0.002	0.153	0.153	115	0.600	0.689	0.49	70460	0.29	TETF
2-7	87	22.6	1.56	40.4	1.447	0.005	0.149	0.149	115	0.596	0.683	0.49	62885	0.29	TETF
2-8	87	20.4	2.18	56.6	1.693	0.016	0.153	0.153	115	0.599	0.677	0.49	56067	0.29	TETF
2-9	87	22.8	2.80	72.7	1.958	0.041	0.150	0.150	115	0.610	0.699	0.50	48806	0.29	TETF
2-10	87	22.7	3.35	87.2	2.212	0.081	0.152	0.152	115	0.580	0.666	0.47	41971	0.29	TETF
2-11	87	23.1	3.97	103.3	2.510	0.151	0.151	0.151	115	0.603	0.703	0.50	38603	0.29	TETF
2-12	87	23.2	4.50	117.1	2.777	0.240	0.155	0.155	115	0.590	0.687	0.48	35276	0.29	TETF
2-13	87	23.2	5.19	134.9	3.135	0.405	0.150	0.055	115	0.635	0.699	0.52	12067	0.29	UTPF
2-14	87	23.5	5.58	145.0	3.345	0.529	0.150	0.055	115	0.642	0.688	0.53	11497	0.29	UTPF
2-15	86	22.9	6.80	176.8	4.032	1.098	0.156	0.020	116	0.642	0.678	0.52	3531	0.29	QLPF
3-1	103	20.4	0.06	1.7	1.007	0.000	0.148	0.148	97	0.834	0.977	0.69	122619	1.81	TF/TETF
3-3	103	22.1	0.35	9.0	1.063	0.000	0.153	0.153	97	0.856	0.963	0.70	123852	1.81	TF/TETF
3-5	103	20.9	0.88	22.9	1.214	0.001	0.139	0.139	97	0.909	1.056	0.78	105460	1.38	TF/TETF
3-7	103	22.3	1.66	43.1	1.486	0.006	0.145	0.145	97	0.892	1.037	0.75	89363	1.38	TF/TETF
3-9	103	22.3	2.86	74.3	1.985	0.045	0.150	0.150	97	0.937	1.066	0.77	74057	1.38	TF/TETF
3-11	103	22.8	4.05	105.2	2.547	0.162	0.148	0.148	97	0.929	1.074	0.77	57495	1.38	TF/TETF
3-13	103	23	5.31	138.0	3.199	0.440	0.149	0.149	97	0.947	1.055	0.78	47881	1.38	TF/TETF
3-14	103	23	5.68	147.7	3.401	0.565	0.145	0.095	97	0.941	1.046	0.79	28677	1.38	LTPF
3-15	103	22.6	6.74	175.2	3.996	1.062	0.149	0.055	97	0.941	0.997	0.78	14348	1.38	LTPF
3-16	103	23.6	7.13	185.5	4.227	1.312	0.150	0.030	97	0.945	0.977	0.78	7472	1.38	UTPF
3-17	103	23.3	7.94	206.6	4.711	1.951	0.149	0.020	97	0.947	1.003	0.78	4532	1.38	QLPF
4-18	87	24.5	8.63	224.3	5.130	2.646	0.146	0.030	115	1.188	1.246	0.99	7906	4.24	UTPF
5-1	75	19.6	0.08	2.0	1.009	0.000	0.134	0.134	133	1.329	1.450	1.16	176789	4.24	TF
5-3	75	21.4	0.36	9.5	1.068	0.000	0.135	0.135	133	1.304	1.437	1.13	165782	4.24	TF
5-5	75	20.2	0.92	23.8	1.225	0.001	0.130	0.130	133	1.363	1.478	1.21	146768	4.24	TF
5-7	75	21.8	1.71	44.4	1.505	0.007	0.134	0.134	133	1.377	1.492	1.20	125898	4.24	TF
5-9	75	21.5	2.89	75.1	1.998	0.047	0.131	0.131	133	1.351	1.473	1.19	92645	4.24	TETF
5-11	75	21.8	4.05	105.4	2.550	0.163	0.130	0.130	133	1.367	1.508	1.21	74217	5.03	TETF
5-13	75	22.3	5.37	139.5	3.231	0.459	0.131	0.131	133	1.385	1.513	1.22	60984	5.03	TETF
5-15	75	22.1	6.76	175.8	4.010	1.076	0.133	0.133	133	1.402	1.533	1.23	51540	5.03	TETF
5-16	75	23	7.20	187.2	4.266	1.356	0.134	0.075	133	1.414	1.526	1.23	27722	5.03	LTPF
5-17	75	22.7	7.76	201.8	4.600	1.790	0.130	0.055	133	1.416	1.501	1.25	19032	5.03	LTPF
5-18	75	23.5	8.51	221.2	5.056	2.512	0.135	0.030	133	1.377	1.425	1.20	9283	5.03	LTPF

The numbering of runs is based on five narrow velocity ranges, sorted from low to high velocity (numbers before hyphen), and up to 18 ranges in clay concentration, sorted from low to high concentration (numbers after hyphen). This numbering system facilitates comparison of flows with similar depth-averaged flow velocity and flows with similar suspended clay concentration.

Note: *T*, mean fluid temperature; *C*, depth-averaged volumetric concentration; η , dynamic viscosity; τ_y , yield strength; *h*, flow depth; *z_p*, height of base of plug flow; *f*(UDVP), (range of) ultrasonic Doppler velocity profiler (UDVP) transducer frequency; *U*, depth-averaged velocity; *U_{max}*, maximum velocity in vertical profile; *Fr*, Froude number; *Re_{TF}*, transitional-flow Reynolds number; TF, turbulent flow; TETF, turbulence-enhanced transitional flow; LTPF, lower transitional plug flow; UTPF, upper transitional plug flow; QLPF, quasi-laminar plug flow.

$$\eta = 0.001 + 0.0992 \left(\frac{C}{100} \right)^{1.2974} \tag{5}$$

$$\tau_y = 22333 \left(\frac{C}{100} \right)^{3.69} \tag{6}$$

where *C* is the depth-averaged volumetric suspended clay concentration at the start of the experiments.

Results

The laboratory experiments with the bentonite flows covered a wide range of flow velocities and volumetric suspended clay concentrations: 0.280–1.418 m s⁻¹ and 0.04–8.63%, respectively. The Froude numbers of these flows ranged from 0.22 (subcritical) to 1.25 (supercritical) (Table 1). Within these ranges, five different clay flow types were distinguished, based on the vertical profiles of downstream velocity and the time-series of the UDVP data (cf. Baas and Best, 2002; Baas *et al.*,

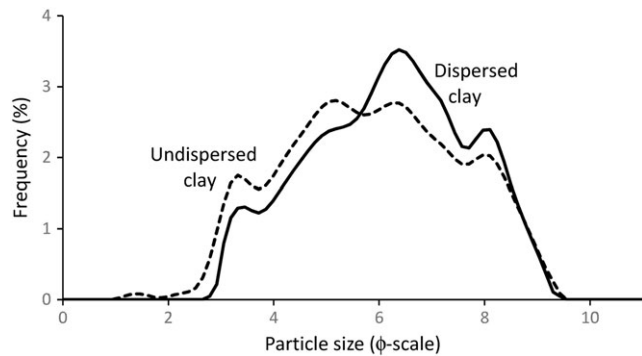


Figure 5. Grain size distribution of the bentonite clay used in the present experiments. Grain size curves for both the undispersed and dispersed (with Calgon) bentonite are shown. Undispersed bentonite: $D_{50} = 0.017$ mm, $\sigma = 1.7$. Dispersed bentonite: $D_{50} = 0.013$ mm, $\sigma = 1.6$. The sorting coefficient, σ , is based on Folk and Ward (1957).

2009). With increasing suspended bentonite concentration, these flow types were:

- 1 *Turbulent flow* (TF) that was characterized by logarithmically-shaped vertical profiles of downstream velocity (Figure 6a) and gradually decreasing $RMS(u')$ and $RMS(u')_0$ with increasing height above the bed (Figures 6b and 6c). In time-series of downstream velocity, TF showed velocity fluctuations on timescales ranging from seconds down to tenths of seconds (Figure 7a). Near-bed values of $RMS(u')$ and $RMS(u')_0$ were low compared to most other flow types (Figures 6b and 6c), and transitional-flow Reynolds numbers ranged from 47,000 to 177,000.
- 2 *Turbulence-enhanced transitional flow* (TETF), which was similar to TF with respect to the logarithmic shape of the vertical profiles of downstream velocity, $RMS(u')$ and $RMS(u')_0$ (Figure 6), and the wide frequency range of fluctuations in at-a-point velocity (Figure 7b). In most runs, however, the time-averaged downstream velocities were lower in magnitude, and the corresponding turbulence intensities were higher, than in TFs of similar suspended sediment concentration (Figure 6). However, the boundary between TF and TETF was poorly defined in the flows with a depth-averaged velocity of approximately 0.92 m s⁻¹. The notation 'TF/TETF' is used in Table I to reflect this uncertainty. Transitional-flow Reynolds numbers in TETF ranged from 26,000 to c. 100,000.
- 3 *Lower-transitional plug flow* (LTPF) that was characterized by high $RMS(u')$ -values close to the bed (Figure 6b) and the presence of a low-turbulence plug region (Figures 6b and 6c), which thickened downward from the water surface as suspended clay concentration was increased. The velocity-time series showed 'saw-tooth'-shaped streamwise velocity fluctuations close to the bed (Figure 7c) and negative spikes of velocity superimposed on a baseline of more constant velocity below the plug flow region (Figure 7d). Transitional-flow Reynolds numbers in LTPF ranged from 9000 to 29,000.
- 4 *Upper-transitional plug flows* (UTPFs), with generally lower $RMS(u')$ -values than LTPFs (Figure 6b), but that also exhibited very low near-bed flow velocities (Figure 6a), which caused $RMS(u')_0$ -values to be similar to, or higher than, in TF and TETF (Figure 6c). Thick plug flow regions characterized the UTPFs, and transitional-flow Reynolds numbers were between 8000 and 12,000 (Table I). In the near-bed velocity time-series, UTPF was characterized by low-amplitude velocity fluctuations with occasional second-scale fluctuations that may possess a 'saw-tooth' shape (Figure 7e).
- 5 *Quasi-laminar plug flow* (QLPF) that is dominated by a thick plug flow region in which downstream velocity is invariant

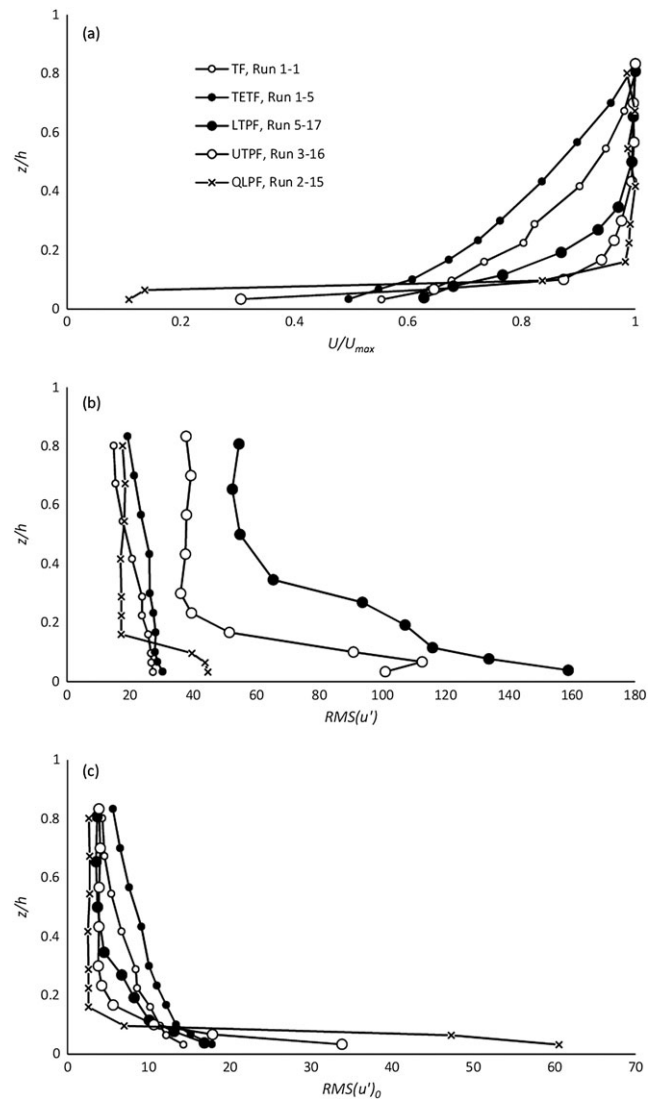


Figure 6. Representative vertical profiles of (a) downstream flow velocity, (b) $RMS(u')$, and (c) $RMS(u')_0$ for bentonite flows. TF, turbulent flow; TETF, turbulence-enhanced transitional flow; LTPF, lower transitional plug flow; UTPF, upper transitional plug flow; QLPF, quasi-laminar plug flow.

with depth (Figures 6b and 6c). The plug flow moved on top of a layer with a steep vertical gradient in velocity (Figure 6a). In general, $RMS(u')$ was low in the plug flow region (Figure 7g), and increased near the bed (Figure 7f). As in UTPF, near-bed $RMS(u')_0$ -values were relatively high in QLPF, because of the presence of very low flow velocities close to the bed (e.g. only 10% of the maximum flow velocity for Run 2–15 in Figure 6a). Transitional-flow Reynolds numbers in QLPF ranged from 3500 to 4500.

Figure 8 depicts changes in near-bed $RMS(u')$ as a function of suspended bentonite concentration for two narrow ranges of depth-averaged flow velocity. Near-bed $RMS(u')$ gradually increased as the clay concentration was increased in TF, TETF and LTPF. After reaching a maximum $RMS(u')$ -value, which appeared to increase with increasing depth-averaged flow velocity, $RMS(u')$ decreased relatively rapidly, as clay concentration increased through UTPF and QLPF.

Interpretations and Discussion

These laboratory experiments reveal predictable changes in the dynamic properties of the bentonite-laden flows that compare

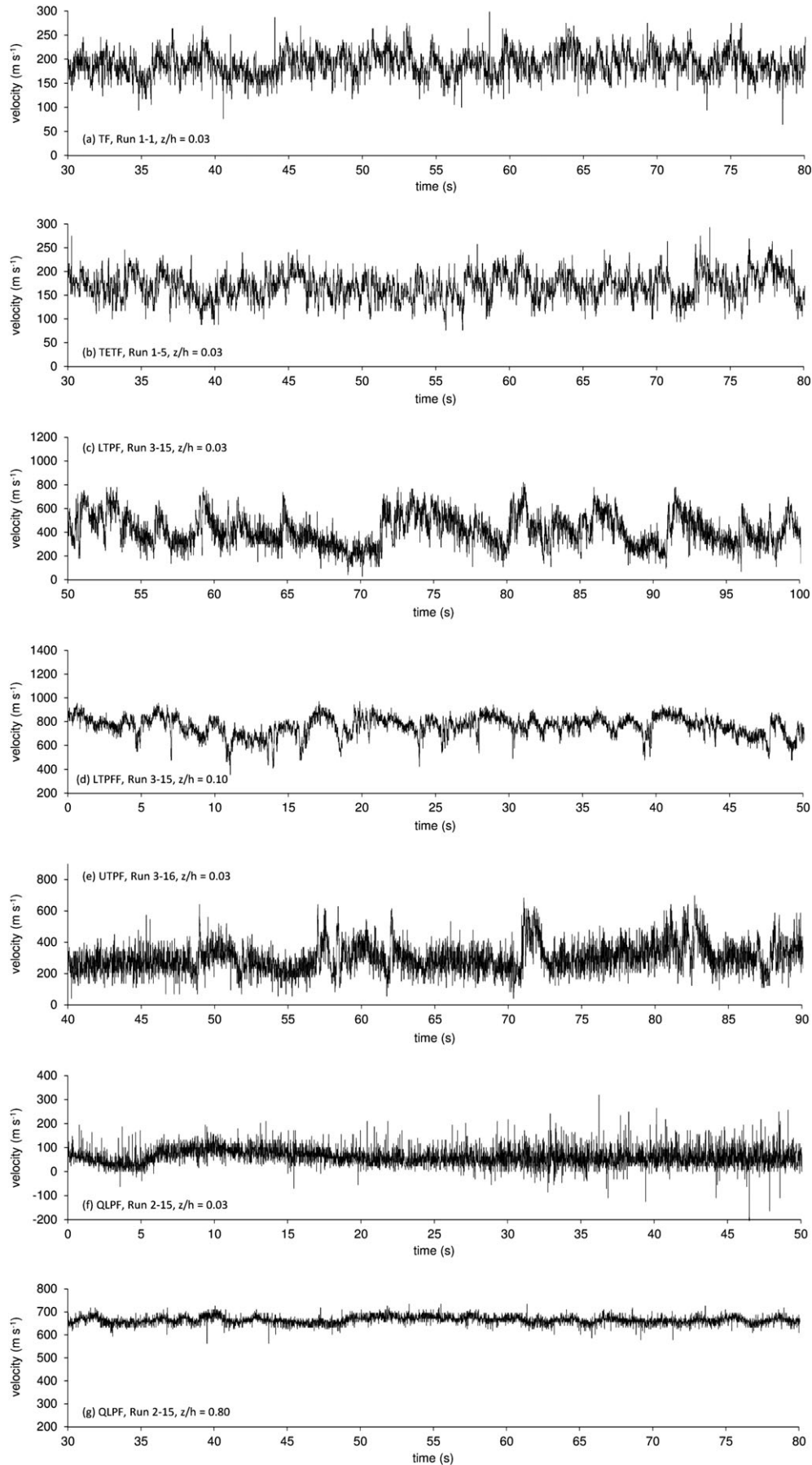


Figure 7. Characteristic time-series of downstream velocity for bentonite flows. (a) Turbulent flow, Run 1–1, $z/h = 0.03$; (b) turbulence-enhanced transitional flow, Run 1–5, $z/h = 0.03$; (c) lower transitional plug flow, Run 3–15, $z/h = 0.03$; (d) lower transitional plug flow, Run 3–15, $z/h = 0.10$; (e) upper transitional plug flow, Run 3–16, $z/h = 0.03$; (f) quasi-laminar plug flow, Run 2–15, $z/h = 0.03$; (f) quasi-laminar plug flow, Run 2–15, $z/h = 0.80$.

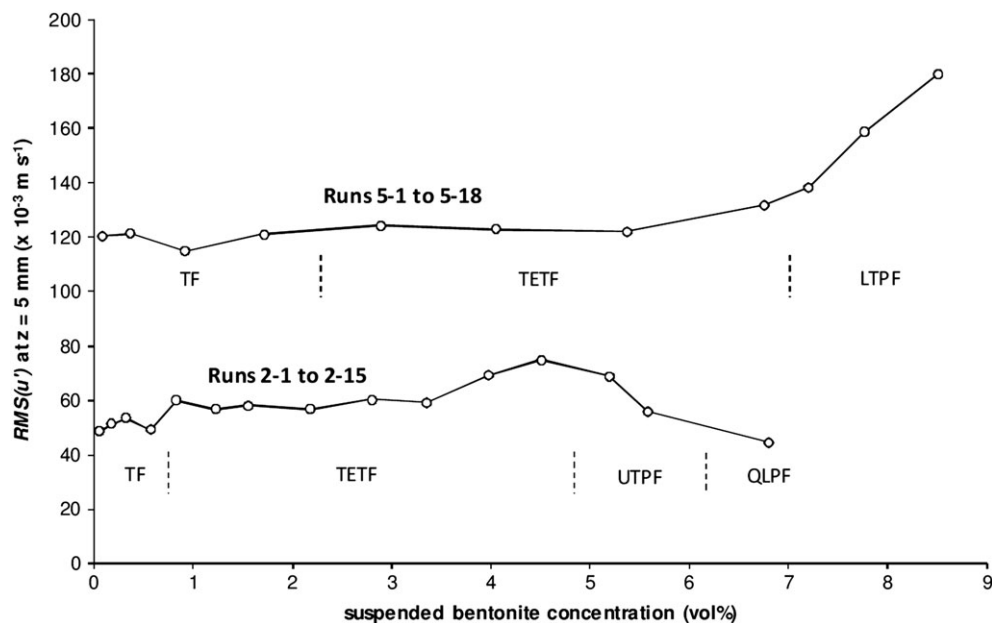


Figure 8. Near-bed $RMS(u')$ plotted against suspended clay concentration in narrow velocity ranges between 0.580 m s^{-1} and 0.642 m s^{-1} (Runs 2–1 to 2–15) and between 1.304 m s^{-1} and 1.416 m s^{-1} (Runs 5–1 to 5–18). TF, turbulent flow; TETF, turbulence-enhanced transitional flow; LTPF, lower transitional plug flow; UTPF, upper transitional plug flow; QLPF, quasi-laminar plug flow.

well with the dynamic properties of kaolinite-laden flows (Baas and Best, 2002; Baas *et al.*, 2009). At low suspended sediment concentrations, both types of clay yield regular turbulent flows, characterized by logarithmic profiles of downstream velocity and turbulence intensity, and fluctuations in velocity on scales ranging from tens of milliseconds to seconds. Laminar plug flows are stable at high suspended bentonite and kaolinite concentrations, with low-intensity turbulence confined to the base of these flows. Moreover, transient TF–QLPF flow behaviour for both bentonite and kaolinite includes (Figure 1): (a) turbulence enhancement at relatively low suspended clay concentrations in TETF; (b) plug flow development, while retaining high near-bed turbulence intensities, in LTPFs; (c) regular velocity fluctuations in LTPFs on the scale of seconds, which become manifested by the progressive attenuation of higher-frequency velocity fluctuations as suspended clay concentration is increased; (d) turbulence attenuation and progressive thickening of the rigid plug in high-concentration UTPFs.

The competing processes of turbulence production and electrostatic binding of clay particles, which have been used to explain the dynamic properties of kaolinite-laden flows (Baas *et al.*, 2009), should therefore also apply to the bentonite-laden flows. Shear-generated turbulence is strong enough to break the cohesive bonds between the bentonite particles in flows that transport this clay at relatively low concentrations, in flows that move at relatively high velocity, and near to the bed where turbulence is generated. Conversely, high suspended bentonite concentrations promote the attenuation of turbulence, and thus allow the bentonite particles to form pervasive gels that move as plug flows. These plug flows expand in a downward direction, as suspended clay concentration is increased and flow velocity is decreased, because it becomes more and more difficult to transfer turbulent kinetic energy into the outer flow regions. Similar to kaolinite flows (Baas and Best, 2002), the presence of near-bed sawtooth shaped velocity fluctuations and negative spikes in streamwise velocity at the base of plug layers in the bentonite flows point to the presence of drag reduction (Best and Leeder, 1993; Baas *et al.*, 2016) and an internal shear layer, in which Kelvin–Helmholtz instabilities provide the additional source of turbulence.

Figure 9 summarizes how turbulence production and clay particle bonds combine to affect the properties of the clay flows by plotting depth-averaged flow velocity against volumetric bentonite concentration and using the recorded hydrodynamic properties to delineate the phase space for turbulent flow, turbulence-enhanced transitional flow, lower and upper transitional plug flow and quasi-laminar plug flow. As expected, the phase boundaries for these flow types climb to higher flow velocities as suspended bentonite concentration is increased, because more kinetic energy is required to break the bonds between the clay particles. In general, this trend corresponds well with the dynamic behaviour of kaolinite flows (Baas *et al.*, 2009). However, the new experimental data show that the phase boundaries for the bentonite flows reside at significantly lower concentrations than for kaolinite flows (Figure 9), particularly at high flow velocities. Only at low flow velocities do the TF–TETF and TETF–LTPF phase boundaries for bentonite and kaolinite flows occur at similar suspended clay concentrations (Figure 9). It can thus be concluded from these data that cohesive forces play a subordinate role at low velocities in TF and TETF where the clay particles are able to form bonds, but that elsewhere in the clay-flow phase diagram it is more difficult to break the bonds between bentonite particles than between kaolinite particles, reflecting the difference in rheological properties of bentonite and kaolinite. Bentonite is a strongly cohesive clay mineral that has a significantly higher molecular viscosity and yield stress than kaolinite, and these differences increase exponentially with increasing suspended clay concentration (Wan, 1982).

Baas *et al.* (2009) showed that the phase boundaries between different turbulent, transitional and laminar kaolinite-laden flows can be described by a narrow range of transitional-flow Reynolds numbers (Figure 3). Figure 10 shows that this observation is also valid for bentonite flows. The boundary between TF and TETF lies at $Re_{TF} = 83,400 \pm 27,300$, $Re_{TF} = 31,000 \pm 10,000$ separates TETF from LTPF, LTPF changes into UTPF at $Re_{TF} = 15,400 \pm 6300$, and QLPF is stable below $Re_{TF} = 6800 \pm 1100$. These Reynolds number thresholds compare well with the thresholds for kaolinite flows (Figure 11). It therefore appears that the transitional-flow Reynolds number is a suitable parameter for delineating turbulent, transitional

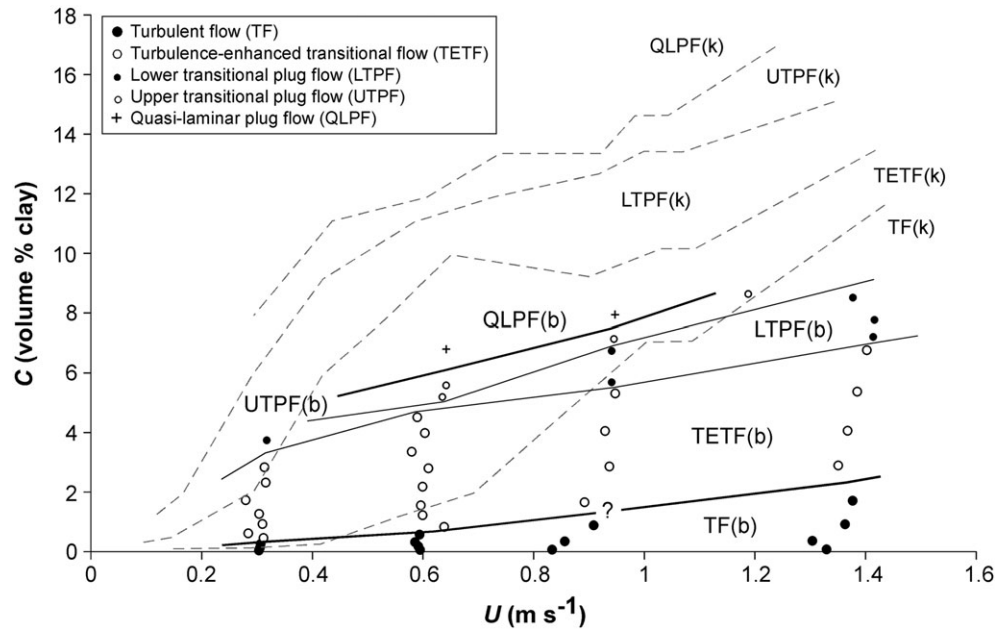


Figure 9. Phase diagram for bentonite flows moving over a flat, smooth, fixed boundary. The phase space for turbulent, transitional, and laminar flows is shown as a function of depth-averaged flow velocity, U , and depth-averaged clay concentration, C . The dashed lines represent the phase boundaries for kaolinite flows. k, kaolinite, b, bentonite.

and laminar flows for different clay minerals. From Equation 2, Table I and from the experimental data of Baas *et al.* (2009), it is possible to deduce that the Re_{TF} -similarity is caused by an approximately constant ratio between flow viscosity and depth-averaged flow velocity. For a given Re_{TF} -value, the higher viscosity in a transitional flow laden with bentonite, when compared to a transitional flow laden with kaolinite, is offset by a higher velocity required to achieve flow behaviour that is similar between the bentonite and kaolinite flows. Since kaolinite and bentonite are common clay minerals that are end members in terms of viscosity and yield stress, it is inferred herein that clay minerals that are more cohesive than kaolinite and less cohesive than bentonite – and other clay minerals within the smectite group – can be described by similar threshold transitional-flow Reynolds numbers. Illite and vermiculite are common clay minerals of intermediate cohesive strength that should fulfil this

reasoning. In Figure 11, four characteristic threshold Re_{TF} -values are proposed, based on integrated data for kaolinite and bentonite, as a guide for discriminating different types of transitional flow in future research and practical applications.

Further Implications

The results of the present study reinforce and extend earlier conclusions (Baas and Best, 2002, 2009; Baas *et al.*, 2009, 2016) that cohesive clay particles can have a substantial effect on the dynamics of Earth-surface flows, even at suspended sediment concentrations that are often considered too low to be able to change flow properties. Bentonite flows should only be turbulent at suspended sediment concentrations below c. 2%, which is equivalent to flow densities of only 1032 kg m^{-3} ,

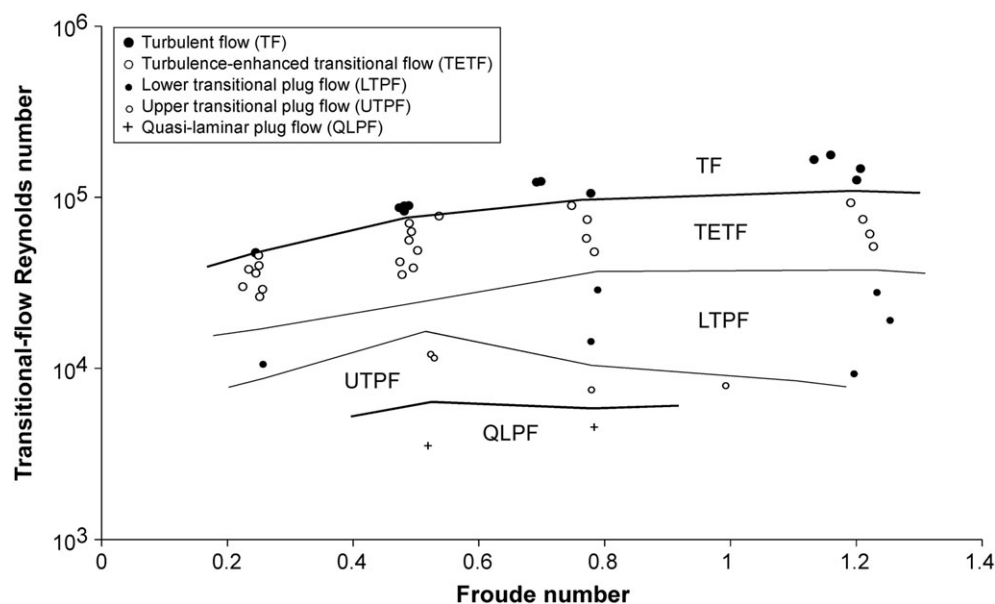


Figure 10. Phase diagram for bentonite flows moving over a flat, smooth, fixed boundary, plotted using the Froude number and transitional-flow Reynolds number. TF, turbulent flow; TETF, turbulence-enhanced transitional flow; LTPF, lower transitional plug flow; UTPF, upper transitional plug flow; QLPF, quasi-laminar plug flow.

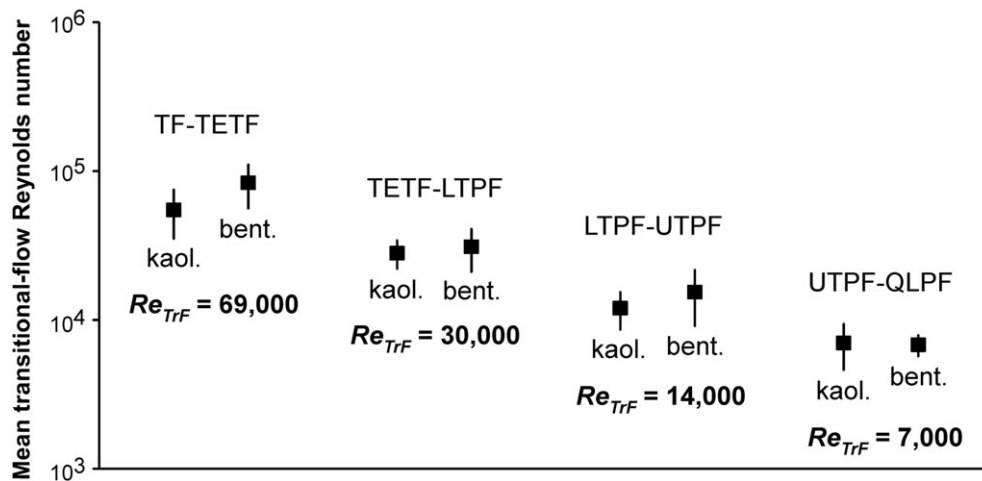


Figure 11. Comparison of mean transitional-flow Reynolds numbers (filled squares) and standard deviations of the mean (vertical lines) for kaolinite and bentonite flows. TF, turbulent flow; TETF, turbulence-enhanced transitional flow; LTPF, lower transitional plug flow; UTPF, upper transitional plug flow; QLPF, quasi-laminar plug flow. The Re_{TrF} -values denote thresholds for turbulent, transitional and laminar flows that are independent of clay type.

i.e. just above the density of seawater. Such densities are common in, for example, flooding rivers, deep-marine turbidity currents, subaerial and subaqueous mudflows, lahars in volcanic environments, and storm-swept estuaries (e.g. Mulder *et al.*, 2003; Alexander *et al.*, 2010; Carling, 2013; Plint, 2014; Talling, 2014). Given the low gradient of the lower and upper phase boundaries of TETF (Figure 9), the threshold concentrations for bentonite-laden TETF and LTPF should thus not be much greater for flows that move faster than the experimental flows herein. Indeed, extrapolating the phase boundary between TF and TETF in Figure 9 by means of linear regression increases the threshold volumetric clay concentration by only 0.8% to 2.8% for flows that move at 5 m s^{-1} . Hence, many natural flows can be expected to experience turbulence enhancement as part of TETF or LTPF. This additional turbulence might lead to an intensification of bed erosion and a capability of these flows to transport larger volumes of sediment, as well as coarser sediment, than classic clearwater turbulent flows. Existing parameterizations for the rate of bed erosion, suspended sediment concentrations in Rouse-type profiles, suspended load transport rate, and bedload transport rate may thus all need revision. Baas *et al.* (2016) provided examples of the substantial influence of cohesive kaolinite on sedimentary bedforms and their primary current stratification, which were in part explained by turbulence modulation. Due to its more cohesive properties, these effects can be expected to be even more dramatic for highly cohesive bentonite, and to commence at much lower clay concentrations in the bed and in the flow. Furthermore, past work on kaolinite flows (Baas and Best, 2008, 2009) has shown how grain and form roughness may also modify the stability fields of the various types of transitional flow through the production of additional form-related turbulence that influences fluid shear, flow mixing and the ability of clays to form bonds and gels. The stability fields of bentonite flows can be expected to be influenced in a similar manner, but again at lower volumetric clay concentrations than for kaolinite flows.

It is also interesting to consider the spatial heterogeneity of clay types in modern environments (e.g. Edzwald and O'Melia, 1975; Weaver, 1990) that is determined by sedimentation and flocculation dynamics, which in turn are controlled by provenance, weathering, and sediment dispersal patterns. Transitional flows may thus affect spatial distributions of sediment that reflect these environmental controls on clay type and abundance. For example, Lasareva and Romankevich (2009) showed that, in the presence of dissolved organic substances, kaolinite and bentonite adopt different coagulation properties

that result in kaolinite being able to cross the river–seawater transition, but in bentonite being unlikely to cross this transition as a result of rapid settling from suspension.

The results presented herein imply that suspended bentonite may have appreciable effects on the properties of sediment-laden flows. Importantly, these effects are felt at lower volumetric clay concentrations than for kaolinite. However, these results still represent an incomplete picture of the complex reality to be found in natural environments. It is well known that salinity may influence the flocculation and gelling behaviour of clays, which may encourage the formation of larger flocs and gels in a shorter period of time compared to freshwater flow. For example, recent work by Gorakhki and Bareither (2015) highlighted the significant influence of salinity on clay suspension behaviour, but also the fact that different clays may behave in different ways to salt concentration and that these effects may be non-linear with changing salinity. It follows that the phase space for transitional flows in natural environments may also be modified by salinity. Moreover, Malarkey *et al.* (2015) and Parsons *et al.* (2016) recently demonstrated the dramatic effects of organic material in the form of extracellular polymeric substances on the development of bedforms, and how these effects may be even more significant than the effect of physical cohesion provided to a sediment bed by clays. Although salinity and biopolymers considerably complicate the phase space of transitional flows, both also further increase the probable occurrence of these flows and their environmental and sedimentological impact. Finally, the results presented herein and in previous work (Baas and Best, 2002, 2008, 2009; Baas *et al.*, 2009) concern purely clay flows that do not also transport silt grade, non-cohesive material in suspension. However, muddy flows transporting both silts and clays may be the norm in many natural flows. The effects of such suspended sediment mixtures require similar experimentation to that presented herein to determine their possible effects on the phase space of transitional flows. Past research and the present results thus all indicate the dramatic effects that clays may have on flow, sediment transport and bed morphology, and highlight the need for new studies, in the laboratory and field, which can more fully quantify the geomorphological and sedimentary consequences of these complex relationships.

Conclusions

Results from laboratory experiments investigating flows laden with suspended bentonite clay moving over a flat bed

demonstrate that the transitional flow behaviour recognized in previous research with kaolinite clay can also be found in bentonite flows, but at lower volumetric suspended clay concentrations. Identical to the previous work on kaolinite flows, five flow regimes can be distinguished, as bentonite concentration is increased: (1) TF; (2) TETF; (3) LTPF; (4) UTPF; (5) QLPF. However, the boundaries between these transitional flow types are reached at lower clay concentrations in bentonite flows, because bentonite attains higher viscosities and yield strengths at far lower volumetric clay concentrations, thus demonstrating an even more dramatic effect on flow properties. The present experiments suggest that bentonite flows should only be fully turbulent at suspended sediment concentrations below c. 2%. The phase space of transitional flows laden with bentonite can be expressed using a Froude number and a transitional-flow Reynolds number, in which the length scale adopted is the thickness of the flow beneath the base of any plug flow. The boundary between TF and TETF is at $Re_{TF}=83,400 \pm 27,300$, $Re_{TF}=31,000 \pm 10,000$ divides TETF from LTPF, LTPF transforms into UTPF at $Re_{TF}=15,400 \pm 6300$, whilst QLPF is stable below $Re_{TF}=6800 \pm 1100$. These values show good agreement with past work on kaolinite-laden suspension flows. Such a transitional-flow Reynolds number criterion may thus be applicable to a wide range of transitional clay flows with viscosities between those of kaolinite and bentonite.

Acknowledgements—The authors are very grateful to the UK Natural Environment Research Council for grant NE/C514823/1 (TransFlow) that enabled this research to be initiated and undertaken at the Sorby Environmental Fluid Dynamics Laboratory, whilst JHB and JLB were at Leeds with JP, and grant NE/I027223/1 (COHBED) that allowed JHB and JP to continue investigating bedform development in mixed cohesive mud and non-cohesive sand. JLB is grateful for a National Great Rivers Research and Education Center Faculty Fellowship that aided the completion of this paper. Gareth Keevil is thanked for his support in the laboratory.

References

- Alexander J, Barclay J, Sušnik J, Loughlin SC, Herd RA, Darnell A, Croswell S. 2010. Sediment-charged flash floods on Montserrat: the influence of synchronous tephra fall and varying extent of vegetation damage. *Journal of Volcanology and Geothermal Research* **194**: 127–138.
- Amos CL, Droppo IG, Gomez EA, Murphy TP. 2003. The stability of a remediated bed in Hamilton Harbour, Lake Ontario, Canada. *Sedimentology* **50**: 149–168.
- Baas JH, Best JL. 2002. Turbulence modulation in clay-rich sediment-laden flows and some implications for sediment deposition. *Journal of Sedimentary Research* **72**: 336–340.
- Baas JH, Best JL. 2008. The dynamics of turbulent, transitional and laminar clay-laden flow over a fixed current ripple. *Sedimentology* **55**: 635–666.
- Baas JH, Best JL. 2009. On the flow of natural clay suspensions over smooth and rough beds. *ERCOFTAC Bulletin* **78**: 32–37.
- Baas JH, Best JL, Peakall J. 2016. Predicting bedforms and primary current stratification in cohesive mixtures of mud and sand. *Journal of the Geological Society* **173**: 12–45. DOI:10.1144/jgs2015-024.
- Baas JH, Best JL, Peakall J, Wang M. 2009. A phase diagram for turbulent, transitional, and laminar clay suspension flows. *Journal of Sedimentary Research* **79**: 162–183.
- Best JL, Leeder MR. 1993. Drag reduction in turbulent muddy seawater flows and some sedimentary consequences. *Sedimentology* **40**: 1129–1137.
- Best JL, Kirkbride AD, Peakall J. 2001. Mean flow and turbulence structure of sediment-laden gravity currents: new insights using ultrasonic Doppler velocity profiling. In *Particulate Gravity Currents*, McCaffrey WD, Kneller BC, Peakall J (eds). IAS Special Publications 31. International Association of Sedimentologists (IAS): Gent; 159–172.
- Caldwell DR, Chriss TM. 1979. The viscous sublayer at the sea floor. *Science* **205**: 1131–1132.
- Carling PA. 2013. Freshwater megaflood sedimentation: what can we learn about generic processes? *Earth-Science Reviews* **125**: 87–113.
- Chang TS, Chun SS. 2012. Micro-characteristics of sustained, fine-grained lacustrine turbidites in the Cretaceous Hwangsan Tuff, SW Korea. *Geosciences Journal* **16**: 409–420.
- Chang TS, Ha HJ, Chun SS. 2015. Factors controlling mud accumulation in the Heuksan mud belt off southwestern Korea. *Geo-Marine Letters* **35**: 461–473. DOI:10.1007/s00367-015-0417-3.
- Coles D. 1956. The law of the wake in the turbulent boundary layer. *Journal of Fluid Mechanics* **1**: 191–226.
- Edzward JK, O'Melia CR. 1975. Clay distributions in recent estuarine sediments. *Clays and Clay Minerals* **23**: 39–44.
- Folk RL, Ward WC. 1957. Brazos River bar, a study in the significance of grain size parameters. *Journal of Sedimentary Petrology* **27**: 3–26.
- Gorakhi MH, Bareither CA. 2015. Salinity effects on sedimentation behaviour of kaolin, bentonite, and soda ash mine tailings. *Applied Clay Science* **114**: 593–602.
- Gust G. 1976. Observations on turbulent-drag reduction in a dilute suspension of clay in sea-water. *Journal of Fluid Mechanics* **75**: 29–47.
- Hansen L, L'Heureux JS, Longva O. 2011. Turbiditic, clay-rich event beds in fjord-marine deposits caused by landslides in emerging clay deposits—palaeoenvironmental interpretation and role for submarine mass-wasting. *Sedimentology* **58**: 890–915.
- Harazim D, McIlroy D. 2015. Mud-rich density-driven flows along an Early Ordovician storm-dominated shoreline: Implications for shallow-marine facies models. *Journal of Sedimentary Research* **85**: 509–528.
- Jablonski BVJ, Dalrymple RW. 2016. Recognition of strong seasonality and climatic cyclicity in an ancient, fluvially dominated, tidally influenced point bar: Middle McMurray Formation, Lower Steepbank River, north-eastern Alberta, Canada. *Sedimentology* **63**: 552–585. DOI:10.1111/sed.12228.
- Kleinhaus MG, Grasmeyer BT. 2006. Bed load transport on the shoreface by currents and waves. *Coastal Engineering* **53**: 983–996.
- La Croix AD, Dashtgard SE. 2014. Of sand and mud: Sedimentological criteria for identifying the turbidity maximum zone in a tidally influenced river. *Sedimentology* **61**: 1961–1981.
- Lasareva EV, Romankevich EA. 2009. Transport of organic matter and clay minerals in estuaries of the Arctic Sea (experimental and field observations). *Oceanology* **49**: 47–54.
- Malarkey J, Baas JH, Hope JA, Aspden RJ, Parsons DR, Peakall J, Paterson DM, Schindler RJ, Ye L, Lichtman ID, Bass SJ, Davies AG, Manning AJ, Thorne PD. 2015. The pervasive role of biological cohesion in bedform development. *Nature Communications* **6**: 6257. DOI:10.1038/ncomms7257.
- Mulder T, Syvitski JPM, Migeon S, Faugeres J-C, Savoye B. 2003. Marine hyperpycnal flows: initiation, behavior and related deposits. A review. *Marine and Petroleum Geology* **20**: 861–882.
- Parsons DR, Schindler RJ, Hope JA, Malarkey J, Baas JH, Peakall J, Manning AJ, Ye L, Simmons S, Paterson DM, Aspden RJ, Bass SJ, Davies AG, Lichtman ID, Thorne PD. 2016. The role of biophysical cohesion on subaqueous bed form size. *Geophysical Research Letters* **43**(4): 1566–1573. DOI:10.1002/2016GL067667.
- Plint AG. 2014. Mud dispersal across a Cretaceous prodelta: Storm-generated, wave-enhanced sediment gravity flows inferred from mudstone microtexture and microfacies. *Sedimentology* **61**: 609–647.
- Sylvester Z, Lowe DR. 2004. Textural trends in turbidites and slurry beds from the Oligocene flysch of the East Carpathians, Romania. *Sedimentology* **51**: 945–972.
- Takeda Y. 1991. Development of an ultrasound velocity profile monitor. *Nuclear Engineering and Design* **126**: 277–284.
- Talling PJ. 2014. On the triggers, resulting flow types and frequencies of subaqueous sediment density flows in different settings. *Marine Geology* **352**: 155–182.
- Van Rijn LC. 1990. Principles of Fluid Flow and Surface Waves in Rivers, Estuaries, Seas and Oceans. Aqua Publications: Amsterdam; 335 pp.
- Wan Z. 1982. Bed Material Movement in Hyperconcentrated Flow, Technical University of Denmark Series Paper 31. Institute of Hydrodynamics and Hydraulic Engineering: Lyngby; 79 pp.
- Wang Z, Plate EJ. 1996. A preliminary study on the turbulence structure of flows of non-Newtonian fluid. *Journal of Hydraulic Research* **34**: 345–361.
- Weaver CE. 1990. Clays, Muds and Shales, Developments in Sedimentology, 44. Elsevier: Amsterdam; 819 pp.